

# $h \rightarrow \mu\tau$ and muon g-2 in the alignment limit of two-Higgs-doublet model

Lei Wang<sup>1</sup>, Shuo Yang<sup>2</sup>, Xiao-Fang Han<sup>1</sup>

<sup>1</sup> *Department of Physics, Yantai University, Yantai 264005, P. R. China*

<sup>2</sup> *Department of Physics, Dalian University, Dalian 116622, P. R. China*

## Abstract

We examine the  $h \rightarrow \mu\tau$  and muon g-2 in the exact alignment limit of two-Higgs-doublet model. In this case, the couplings of the SM-like Higgs to the SM particles are the same as the Higgs couplings in the SM at the tree level, and the tree-level lepton-flavor-violating coupling  $h\mu\tau$  is absent. We assume the lepton-flavor-violating  $\mu\tau$  excess observed by CMS to be respectively from the other neutral Higgses,  $H$  and  $A$ , which almost degenerates with the SM-like Higgs at the 125 GeV. After imposing the relevant theoretical constraints and experimental constraints from the precision electroweak data,  $B$ -meson decays,  $\tau$  decays and Higgs searches, we find that the muon g-2 anomaly and  $\mu\tau$  excess favor the small lepton Yukawa coupling and top Yukawa coupling of the non-SM-like Higgs around 125 GeV, and the lepton-flavor-violating coupling is sensitive to another heavy neutral Higgs mass. In addition, if the  $\mu\tau$  excess is from  $H$  around 125 GeV, the experimental data of the heavy Higgs decaying into  $\mu\tau$  favor  $m_A > 230$  GeV for a relatively large  $H\bar{t}t$  coupling.

PACS numbers: 12.60.Fr, 14.80.Ec, 14.80.Bn

## I. INTRODUCTION

The ATLAS and CMS collaborations have probed the lepton-flavor-violating (LFV) Higgs decay  $h \rightarrow \mu\tau$  around 125 GeV at the LHC run-I [1–3] and early run-II [4]. By the analysis of data sample corresponding to an integrated luminosity of  $20.3 \text{ fb}^{-1}$  at the  $\sqrt{s} = 8 \text{ TeV}$  LHC, the ATLAS Collaboration found a mild deviation of  $1\sigma$  significance in the  $h \rightarrow \mu\tau$  channel and set an upper limit of  $Br(h \rightarrow \mu\tau) < 1.43\%$  at 95% confidence level with a best fit  $Br(h \rightarrow \mu\tau) = (0.53 \pm 0.51)\%$  [2]. Based on the data sample corresponding to an integrated luminosity of  $19.7 \text{ fb}^{-1}$  at the  $\sqrt{s} = 8 \text{ TeV}$  LHC, the CMS collaboration imposed an upper limit of  $Br(h \rightarrow \mu\tau) < 1.51\%$  at 95% confidence level, while the best fit value is  $Br(h \rightarrow \mu\tau) = (0.84^{+0.39}_{-0.37})\%$  with a small excess of  $2.4\sigma$  [3]. At the  $\sqrt{s} = 13 \text{ TeV}$  LHC run-II with an integrated luminosity of  $2.3 \text{ fb}^{-1}$ , the CMS collaboration did not observe the excess and imposed an upper limit of  $Br(h \rightarrow \mu\tau) < 1.2\%$  [4]. However, the CMS search result at the early LHC run-II can not definitely kill the excess of  $h \rightarrow \mu\tau$  due to the low integrated luminosity.

If the  $h \rightarrow \mu\tau$  excess is not a statistical fluctuation, the new physics with the LFV interactions can give a simple explanation for the excess. On the other hand, the long-standing anomaly of the muon anomalous magnetic moment (muon g-2) implies that the new physics is connected to muons. The two excesses can be simultaneously explained by the LFV Higgs interactions, such as the general two-Higgs-doublet model (2HDM) with the LFV Higgs interactions. There have been many studies on the  $h \rightarrow \mu\tau$  excess in the framework of 2HDM [5–7] and some other new physics models [8].

In this paper, we discuss the excesses of  $h \rightarrow \mu\tau$  and muon g-2 in the exact alignment limit of the general 2HDM where one of the neutral Higgs mass eigenstates is aligned with the direction of the scalar field vacuum expectation value (VEV) [9]. In the interesting scenario, the SM-like Higgs couplings to the SM particles are the same as the Higgs couplings in the SM at the tree level, and the tree-level LFV coupling  $h\mu\tau$  is absent. We assume the  $\mu\tau$  excess observed by CMS to be respectively from the other neutral Higgses,  $H$  and  $A$ , which almost degenerates with the SM-like Higgs at the 125 GeV. In our discussions, we impose the relevant theoretical constraints from the vacuum stability, unitarity and perturbativity as well as the experimental constraints from the precision electroweak data,  $B$ -meson decays,  $\tau$  decays and Higgs searches.

Our work is organized as follows. In Sec. II we recapitulate the alignment limit of 2HDM. In Sec. III we perform the numerical calculations and discuss the muon g-2 anomaly and the  $\mu\tau$  excess around 125 GeV after imposing the relevant theoretical and experimental constraints. Finally, we give our conclusion in Sec. IV.

## II. TWO-HIGGS-DOUBLET MODEL AND THE ALIGNMENT LIMIT

The alignment limit of 2HDM is defined as the limit in which one of the two neutral CP-even Higgs mass eigenstates aligns with the direction of the scalar field VEV [9]. The alignment limit can be easily realized in the decoupling limit [10], namely that all the non-SM-like Higgses are very heavy. The possibility of alignment without decoupling limit was first noted in [10], "re-invented" in [11–13] and further studied in [9, 14–17]. The alignment limit is basis-independent, and clearly exhibited in the Higgs basis. The alignment limit also exists in the Minimal Supersymmetric Standard Model which is a constrained incarnation of the general 2HDM. There are some detailed discussions in [18, 19] and a very recent study in [20].

### A. Two-Higgs-doublet model in the Higgs basis

The general Higgs potential is written as [21]

$$\begin{aligned}
V = & \mu_1(H_1^\dagger H_1) + \mu_2(H_2^\dagger H_2) + \left[ \mu_3(H_1^\dagger H_2 + \text{h.c.}) \right] \\
& + \frac{k_1}{2}(H_1^\dagger H_1)^2 + \frac{k_2}{2}(H_2^\dagger H_2)^2 + k_3(H_1^\dagger H_1)(H_2^\dagger H_2) + k_4(H_1^\dagger H_2)(H_2^\dagger H_1) \\
& + \left[ \frac{k_5}{2}(H_1^\dagger H_2)^2 + \text{h.c.} \right] + \left[ k_6(H_1^\dagger H_1)(H_1^\dagger H_2) + \text{h.c.} \right] \\
& + \left[ k_7(H_2^\dagger H_2)(H_1^\dagger H_2) + \text{h.c.} \right].
\end{aligned} \tag{1}$$

All  $\mu_i$  and  $k_i$  are real in the CP-conserving case. In the Higgs basis, the  $H_1$  field has a VEV  $v = 246$  GeV, and the VEV of  $H_2$  field is zero. The two complex scalar doublets have the hypercharge  $Y = 1$ ,

$$H_1 = \begin{pmatrix} G^+ \\ \frac{1}{\sqrt{2}}(v + \rho_1 + iG_0) \end{pmatrix}, \quad H_2 = \begin{pmatrix} H^+ \\ \frac{1}{\sqrt{2}}(\rho_2 + iA_0) \end{pmatrix}. \tag{2}$$

The Nambu-Goldstone bosons  $G^0$  and  $G^\pm$  are eaten by the gauge bosons. The  $H^\pm$  and  $A$  are the mass eigenstates of the charged Higgs boson and CP-odd Higgs boson, and their masses are given by

$$m_A^2 = m_{H^\pm}^2 + \frac{1}{2}v^2(k_4 - k_5). \quad (3)$$

The physical CP-even Higgs bosons  $h$  and  $H$  are the linear combinations of  $\rho_1$  and  $\rho_2$ ,

$$\begin{pmatrix} \rho_1 \\ \rho_2 \end{pmatrix} = \begin{pmatrix} s_\theta & c_\theta \\ c_\theta & -s_\theta \end{pmatrix} \begin{pmatrix} h \\ H \end{pmatrix}, \quad (4)$$

and their masses are given as

$$m_{h,H}^2 = \frac{1}{2} \left[ m_A^2 + (k_1 + k_5)v^2 \mp \sqrt{[m_A^2 + (k_5 - k_1)v^2]^2 + 4k_6^2v^4} \right]. \quad (5)$$

Where  $s_\theta \equiv \sin \theta$  and  $c_\theta \equiv \cos \theta$ ,

$$\cos \theta = \frac{-k_6v^2}{\sqrt{(m_H^2 - m_h^2)(m_H^2 - k_1v^2)}}. \quad (6)$$

In this paper we take the light CP-even Higgs  $h$  as the 125 GeV Higgs. For  $\cos \theta = 0$ , the mass eigenstates of CP-even Higgs bosons are obtained from the Eq. (4),

$$h = \rho_1, \quad H = -\rho_2, \quad (7)$$

which is so called "alignment limit". The Eq. (6) shows that the alignment limit can be realized in two ways:  $k_6 = 0$  or  $m_H^2 \gg v^2$ . The latter is called the decoupling limit. In this paper we focus on the former, which is the alignment without decoupling limit. In the alignment limit, the  $h$  couplings to gauge bosons are the same as the Higgs couplings in the SM, and the  $H$  has no couplings to gauge bosons.

## B. The Higgs couplings

We can rotate the Higgs basis by a mixing angle  $\beta$ ,

$$\begin{pmatrix} \Phi_1 \\ \Phi_2 \end{pmatrix} = \begin{pmatrix} c_\beta & -s_\beta \\ s_\beta & c_\beta \end{pmatrix} \begin{pmatrix} H_1 \\ H_2 \end{pmatrix}. \quad (8)$$

Where  $s_\beta \equiv \sin \beta$ ,  $c_\beta \equiv \cos \beta$ , and  $\tan \beta = v_2/v_1$  with  $v_2$  and  $v_1$  being the VEVs of  $\Phi_2$  and  $\Phi_1$  and  $v^2 = v_1^2 + v_2^2 = (246 \text{ GeV})^2$ .

The general Higgs potential is written as [21]

$$\begin{aligned}
V = & m_{11}^2(\Phi_1^\dagger\Phi_1) + m_{22}^2(\Phi_2^\dagger\Phi_2) - \left[ m_{12}^2(\Phi_1^\dagger\Phi_2 + \text{h.c.}) \right] \\
& + \frac{\lambda_1}{2}(\Phi_1^\dagger\Phi_1)^2 + \frac{\lambda_2}{2}(\Phi_2^\dagger\Phi_2)^2 + \lambda_3(\Phi_1^\dagger\Phi_1)(\Phi_2^\dagger\Phi_2) + \lambda_4(\Phi_1^\dagger\Phi_2)(\Phi_2^\dagger\Phi_1) \\
& + \left[ \frac{\lambda_5}{2}(\Phi_1^\dagger\Phi_2)^2 + \text{h.c.} \right] + \left[ \lambda_6(\Phi_1^\dagger\Phi_1)(\Phi_1^\dagger\Phi_2) + \text{h.c.} \right] \\
& + \left[ \lambda_7(\Phi_2^\dagger\Phi_2)(\Phi_1^\dagger\Phi_2) + \text{h.c.} \right].
\end{aligned} \tag{9}$$

The parameters  $m_{ij}$  and  $\lambda_i$  are the linear combinations of the parameters in the Higgs basis:  $\mu_i$  and  $k_i$ . The detailed expressions are introduced in [9, 22]. After spontaneous electroweak symmetry breaking, there are five physical Higgses: two neutral CP-even  $h$  and  $H$ , one neutral pseudoscalar  $A$ , and two charged scalar  $H^\pm$ .

The general Yukawa interaction can be given as

$$\begin{aligned}
-\mathcal{L} = & Y_{u1} \overline{Q}_L \tilde{\Phi}_1 u_R + Y_{d1} \overline{Q}_L \Phi_1 d_R + Y_{\ell 1} \overline{L}_L \Phi_1 e_R \\
& + Y_{u2} \overline{Q}_L \tilde{\Phi}_2 u_R + Y_{d2} \overline{Q}_L \Phi_2 d_R + Y_{\ell 2} \overline{L}_L \Phi_2 e_R + \text{h.c.},
\end{aligned} \tag{10}$$

where  $Q_L^T = (u_L, d_L)$ ,  $L_L^T = (\nu_L, l_L)$ ,  $\tilde{\Phi}_{1,2} = i\tau_2 \Phi_{1,2}^*$ , and  $Y_{u1,2}$ ,  $Y_{d1,2}$  and  $Y_{\ell 1,2}$  are  $3 \times 3$  matrices in family space.

To avoid the tree-level FCNC couplings of the quarks, we take

$$\begin{aligned}
Y_{u1} &= c_u \rho_u, & Y_{u2} &= s_u \rho_u, \\
Y_{d1} &= c_d \rho_d, & Y_{d2} &= s_d \rho_d,
\end{aligned} \tag{11}$$

where  $c_u \equiv \cos \theta_u$ ,  $s_u \equiv \sin \theta_u$ ,  $c_d \equiv \cos \theta_d$ ,  $s_d \equiv \sin \theta_d$  and  $\rho_u$  ( $\rho_d$ ) is the  $3 \times 3$  matrix. For this choice, the interaction corresponds to the aligned 2HDM [23, 24].

For the Yukawa coupling matrix of the lepton, we take

$$\begin{aligned}
X_{ii} &= \frac{\sqrt{2}m_{\ell_i}}{v}(s_\beta + c_\beta \kappa_\ell), \\
X_{\tau\mu} &= c_\beta \rho_{\tau\mu}, \\
X_{\mu\tau} &= c_\beta \rho_{\mu\tau}.
\end{aligned} \tag{12}$$

Where  $X = V_L Y_{\ell 2} V_R^\dagger$ , and  $V_L$  ( $V_R$ ) is the unitary matrix which transforms the interaction eigenstates to the mass eigenstates of the left-handed (right-handed) lepton fields. The other nondiagonal matrix elements of  $X$  are zero.

The Yukawa couplings of the neutral Higgs bosons are given as

$$\begin{aligned}
y_{hf_i f_i} &= \frac{m_{f_i}}{v} [\sin(\beta - \alpha) + \cos(\beta - \alpha)\kappa_f], \\
y_{Hf_i f_i} &= \frac{m_{f_i}}{v} [\cos(\beta - \alpha) - \sin(\beta - \alpha)\kappa_f], \\
y_{Af_i f_i} &= -i\frac{m_{f_i}}{v}\kappa_f \text{ (for u)}, \quad y_{Af_i f_i} = i\frac{m_{f_i}}{v}\kappa_f \text{ (for d, } \ell), \\
y_{h\tau\mu} &= \cos(\beta - \alpha)\frac{\rho_{\tau\mu}}{\sqrt{2}}, \quad y_{h\mu\tau} = \cos(\beta - \alpha)\frac{\rho_{\mu\tau}}{\sqrt{2}}, \\
y_{H\tau\mu} &= -\sin(\beta - \alpha)\frac{\rho_{\tau\mu}}{\sqrt{2}}, \quad y_{H\mu\tau} = -\sin(\beta - \alpha)\frac{\rho_{\mu\tau}}{\sqrt{2}}, \\
y_{A\tau\mu} &= i\frac{\rho_{\tau\mu}}{\sqrt{2}}, \quad y_{A\mu\tau} = i\frac{\rho_{\mu\tau}}{\sqrt{2}}.
\end{aligned} \tag{13}$$

Where  $\kappa_u \equiv -\tan(\beta - \theta_u)$ ,  $\kappa_d \equiv -\tan(\beta - \theta_d)$ . The  $\kappa_\ell$  is a free input parameter, which is used to parameterize the matrix element of the lepton Yukawa coupling, as shown in Eq. (12). In other words, the matrix elements of the lepton Yukawa coupling are taken as the Eq. (12) in order to obtain the Yukawa couplings of lepton in Eq. (13).

The neutral Higgs bosons couplings to the gauge bosons normalized to the SM Higgs boson are given by

$$y_V^h = \sin(\beta - \alpha), \quad y_V^H = \cos(\beta - \alpha), \tag{14}$$

where  $V$  denotes  $Z$  and  $W$ .

In the exact alignment limit, namely  $\cos(\beta - \alpha) = 0$ , the Eq. (13) and Eq. (14) show that the 125 GeV Higgs ( $h$ ) has the same couplings to the fermions and gauge bosons as the SM values, and the tree-level LFV couplings are absent. The heavy CP-even Higgs ( $H$ ) has no coupling to the gauge bosons, and there are the tree-level LFV couplings for the  $A$  and  $H$ .

### III. NUMERICAL CALCULATIONS AND DISCUSSIONS

#### A. Numerical calculations

In the exact alignment limit, the SM-like Higgs has no tree-level LFV coupling. In order to explain the  $h \rightarrow \mu\tau$  excess reported by CMS, we assume the signal to be respectively from  $H$  and  $A$ , which almost degenerates with the SM-like Higgs at the 125 GeV. Here we take two scenarios simply: (i)  $m_A=126$  GeV and (ii)  $m_H=126$  GeV.

In our calculations, the other involved parameters are randomly scanned in the following ranges:

$$\begin{aligned}
& -(400 \text{ GeV})^2 \leq m_{12}^2 \leq (400 \text{ GeV})^2, \quad 0.1 \leq \tan \beta \leq 10, \\
& 100 \text{ GeV} \leq m_{H^\pm} \leq 700 \text{ GeV}, \\
& 0 \leq \kappa_u \leq 1.2, \quad -150 \leq \kappa_\ell \leq 150, \quad -0.3 \leq \rho_{\tau\mu} \leq 0.3 \\
& \text{Scenario i : } m_A = 126 \text{ GeV}, \quad 150 \text{ GeV} \leq m_H \leq 700 \text{ GeV}, \quad \rho_{\mu\tau} = -\rho_{\tau\mu}, \\
& \text{Scenario ii : } m_H = 126 \text{ GeV}, \quad 150 \text{ GeV} \leq m_A \leq 700 \text{ GeV}, \quad \rho_{\mu\tau} = \rho_{\tau\mu}. \quad (15)
\end{aligned}$$

In order to relax the constraints from the observables of down-type quarks, we take  $\kappa_d = 0$ . For the cases of  $m_A = 126 \text{ GeV}$  and  $m_H = 126 \text{ GeV}$ , we respectively take  $\rho_{\mu\tau} = -\rho_{\tau\mu}$  and  $\rho_{\mu\tau} = \rho_{\tau\mu}$  to produce a large positive contribution to the muon g-2. The pseudoscalar  $A$  can give the positive contributions to the muon g-2 via the two-loop Barr-Zee diagrams with the lepton-flavor-conserving (LFC) coupling. Therefore, we take  $|\kappa_\ell| < 150$  to examine the possibility of explaining the muon g-2. In the exact alignment limit, the  $h\tau\bar{\tau}$  coupling is independent on  $\kappa_\ell$  and equals the SM value. However, the  $A\tau\bar{\tau}$  and  $H\tau\bar{\tau}$  couplings can reach 1.08 and be slightly larger than 1 for  $|\kappa_\ell| = 150$ , which can not lead to the problem on the perturbativity due to the suppression of the loop factor. In addition, for such large  $\kappa_\ell$  the  $Br(A \rightarrow \tau\bar{\tau})$  and  $Br(H \rightarrow \tau\bar{\tau})$  can reach 1. Due to  $\kappa_d = 0$  and  $\cos(\beta - \alpha) = 0$ , the cross sections of  $A$  and  $H$  are equal to zero in the  $b\bar{b}$  associated production mode and vector boson fusion production mode. However, the searches for  $gg \rightarrow A/H \rightarrow \tau\bar{\tau}$  can give the constraints on  $\kappa_u$ . We will discuss the constraints in the following item (5).

During the scan, we consider the following experimental constraints and observables:

**(1) Theoretical constraints and precision electroweak data.** We use 2HDMC-1.6.5 [25] to implement the theoretical constraints from the vacuum stability, unitarity and coupling-constant perturbativity, as well as the constraints from the oblique parameters ( $S, T, U$ ) and  $\delta\rho$ .

**(2)  $B$ -meson decays and  $R_b$ .** Although the tree-level FCNCs in the quark sector are absent, they will appear at the one-loop level in this model. We consider the constraints of  $B$ -meson decays from  $\Delta m_{B_s}$ ,  $\Delta m_{B_d}$ ,  $B \rightarrow X_s \gamma$ , and  $B_s \rightarrow \mu^+ \mu^-$ , which are respectively calculated using the formulas in [26–28]. In addition, we consider the  $R_b$  constraints, which is calculated following the formulas in [29]. In fact, in this paper we take  $\kappa_d = 0$  and  $0 \leq \kappa_u \leq 1.2$ , which will relax the constraints from the bottom-quark observables sizably.

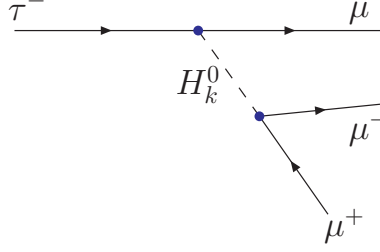


FIG. 1: The main Feynman diagrams of  $\tau^- \rightarrow \mu^- \mu^- \mu^+$ . The two  $\mu^-$  in final states can be exchanged. In the exact alignment limit  $H_k^0$  denotes  $A$  and  $H$ .

**(3)  $\tau$  decays.** In this model, the non-SM-like Higgses have the tree-level LFV couplings to  $\tau$  lepton, and the LFC couplings to lepton can be sizably enhanced for  $-150 \leq \kappa_\ell \leq 150$ . Therefore, some  $\tau$  decay processes can give very strong constraints on the model.

- (i)  $\tau \rightarrow 3\mu$ . In the exact alignment limit, the LFV  $A\tau\mu$  and  $H\tau\mu$  couplings generate the  $\tau \rightarrow \mu^+ \mu^- \mu^-$  process at the tree level, and the corresponding Feynman diagrams are shown in Fig. 1. The branching ratio of  $\tau \rightarrow 3\mu$  is given as [30]

$$\frac{Br(\tau \rightarrow 3\mu)}{Br(\tau \rightarrow \mu \bar{\nu} \nu)} = \sum_{\phi_1, \phi_2 = A, H} \frac{I(\phi_1, \phi_2)}{64G_F^2}, \quad (16)$$

where

$$\begin{aligned} I(\phi_1, \phi_2) = & 2 \frac{y_{\phi_1 \mu \tau} y_{\phi_1 \mu \mu}^*}{m_{\phi_1}^2} \frac{y_{\phi_2 \mu \tau} y_{\phi_2 \mu \mu}^*}{m_{\phi_2}^2} + 2 \frac{y_{\phi_1 \tau \mu} y_{\phi_1 \mu \mu}^*}{m_{\phi_1}^2} \frac{y_{\phi_2 \tau \mu} y_{\phi_2 \mu \mu}^*}{m_{\phi_2}^2} \\ & + \frac{y_{\phi_1 \mu \tau} y_{\phi_1 \mu \mu}^*}{m_{\phi_1}^2} \frac{y_{\phi_2 \mu \tau} y_{\phi_2 \mu \mu}^*}{m_{\phi_2}^2} + \frac{y_{\phi_1 \tau \mu} y_{\phi_1 \mu \mu}^*}{m_{\phi_1}^2} \frac{y_{\phi_2 \tau \mu} y_{\phi_2 \mu \mu}^*}{m_{\phi_2}^2}. \end{aligned} \quad (17)$$

The current experimental upper bound of  $Br(\tau \rightarrow 3\mu)$  is [31],

$$Br(\tau \rightarrow 3\mu) < 2.1 \times 10^{-8}. \quad (18)$$

From the Eq. (17), we can find that the experimental data of  $Br(\tau \rightarrow 3\mu)$  will give the very strong constraints on the products,  $\rho_{\tau\mu} \times \kappa_\ell$  and  $\rho_{\mu\tau} \times \kappa_\ell$ .

- (ii)  $\tau \rightarrow \mu\gamma$ . The main Feynman diagrams of  $\tau \rightarrow \mu\gamma$  in the model are shown in Fig. 2. In the exact alignment limit, the SM-like Higgs has no tree-level LFV coupling, and the heavy CP-even Higgs couplings to the gauge bosons are equal to zero. Therefore, the SM-like Higgs does not contribute to the  $\tau \rightarrow \mu\gamma$ , and the  $\tau \rightarrow \mu\gamma$  can not be



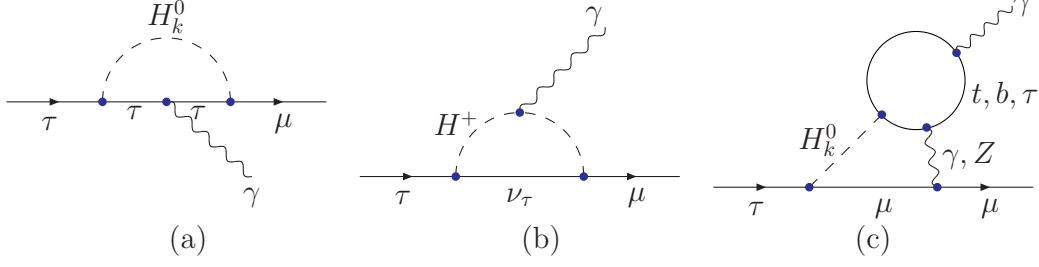


FIG. 2: The main Feynman diagrams of  $\tau \rightarrow \mu\gamma$ . In the exact alignment limit  $H_k^0$  denotes  $A$  and  $H$ .

corrected via the two-loop Barr-Zee diagrams with the  $W$  loop. The  $Br(\tau \rightarrow \mu\gamma)$  in this model is given by

$$\frac{\text{BR}(\tau \rightarrow \mu\gamma)}{\text{BR}(\tau \rightarrow \mu\bar{\nu}\nu)} = \frac{48\pi^3\alpha (|A_{1L0} + A_{1Lc} + A_{2L}|^2 + |A_{1R0} + A_{1Rc} + A_{2R}|^2)}{G_F^2}, \quad (19)$$

where  $A_{1L0}$ ,  $A_{1Lc}$ ,  $A_{1R0}$  and  $A_{1Rc}$  are from the one-loop diagrams with the Higgs boson and  $\tau$  lepton [6],

$$A_{1L0} = \sum_{\phi=H, A} \frac{y_{\phi\tau\mu}^*}{16\pi^2 m_\phi^2} \left[ y_{\phi\tau\tau}^* \left( \log \frac{m_\phi^2}{m_\tau^2} - \frac{3}{2} \right) + \frac{y_{\phi\tau\tau}}{6} \right], \quad (20)$$

$$A_{1Lc} = -\frac{(\rho^{e\dagger}\rho^e)^{\mu\tau}}{192\pi^2 m_{H^-}^2}, \quad (21)$$

$$A_{1R0} = A_{1L0} (y_{\phi\tau\mu}^* \rightarrow y_{\phi\mu\tau}, \quad y_{\phi\tau\tau} \leftrightarrow y_{\phi\tau\tau}^*), \quad (22)$$

$$A_{1Rc} = 0. \quad (23)$$

The  $A_{2L}$  and  $A_{2R}$  are from the two-loop Barr-Zee diagrams with the third-generation fermion loop [6],

$$\begin{aligned} A_{2L} &= - \sum_{\phi=H, A; f=t, b, \tau} \frac{N_C Q_f \alpha}{8\pi^3} \frac{y_{\phi\tau\mu}^*}{m_\tau m_f} [Q_f \{ \text{Re}(y_{\phi ff}) F_H(x_{f\phi}) - i \text{Im}(y_{\phi ff}) F_A(x_{f\phi}) \} \\ &\quad + \frac{(1 - 4s_W^2)(2T_{3f} - 4Q_f s_W^2)}{16s_W^2 c_W^2} \left\{ \text{Re}(y_{\phi ff}) \tilde{F}_H(x_{f\phi}, x_{fZ}) - i \text{Im}(y_{\phi ff}) \tilde{F}_A(x_{f\phi}, x_{fZ}) \right\} ], \\ A_{2R} &= A_{2L} (y_{\phi\tau\mu}^* \rightarrow y_{\phi\mu\tau}, \quad i \rightarrow -i), \end{aligned} \quad (24)$$

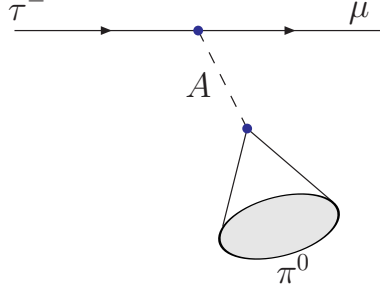


FIG. 3: The main Feynman diagram of  $\tau \rightarrow \mu\pi^0$ .

where  $T_{3f}$  denotes the isospin of the fermion, and

$$\begin{aligned}
F_H(y) &= \frac{y}{2} \int_0^1 dx \frac{1 - 2x(1-x)}{x(1-x) - y} \log \frac{x(1-x)}{y} \quad (\text{for } \phi = H), \\
F_A(y) &= \frac{y}{2} \int_0^1 dx \frac{1}{x(1-x) - y} \log \frac{x(1-x)}{y} \quad (\text{for } \phi = A), \\
\tilde{F}_H(x, y) &= \frac{x F_H(y) - y F_H(x)}{x - y}, \\
\tilde{F}_A(x, y) &= \frac{x F_A(y) - y F_A(x)}{x - y}.
\end{aligned} \tag{25}$$

The two terms of  $A_{2L}$  come from the effective  $\phi\gamma\gamma$  vertex and  $\phi Z\gamma$  vertex induced by the third-generation fermion loop. The current experimental data give an upper bound of  $Br(\tau \rightarrow \mu\gamma)$  [33],

$$Br(\tau \rightarrow \mu\gamma) < 4.4 \times 10^{-8}. \tag{26}$$

- (iii)  $\tau \rightarrow \mu\pi^0$ . The  $\tau$  can decay into a lepton and a pseudoscalar meson at the tree level via the CP-odd Higgs with the LFV couplings, such as  $\tau \rightarrow \mu\pi^0$ . The corresponding Feynman diagrams are shown in Fig. 3. The width of  $\tau \rightarrow \mu\pi^0$  is given as [34],

$$\Gamma(\tau \rightarrow \mu\pi^0) = \frac{f_\pi^2 m_\pi^4 m_\tau}{512 \pi m_A^4 v^2} (|\rho_{\tau\mu}|^2 + |\rho_{\mu\tau}|^2) (\kappa_u + \kappa_d)^2. \tag{27}$$

The current upper bound of  $Br(\tau \rightarrow \mu\pi^0)$  is [35],

$$Br(\tau \rightarrow \mu\pi^0) < 1.1 \times 10^{-7}. \tag{28}$$

**(4) muon g-2.** The dominant contributions to the muon g-2 are from the one-loop diagrams with the Higgs LFV coupling [36], and the corresponding Feynman diagrams can

be obtained by replacing the initial states  $\tau$  with  $\mu$  in Fig. 2 (a) and Fig. 2 (b). In the exact alignment limit,

$$\delta a_{\mu 1}^{LFV} = \frac{m_\mu m_\tau \rho_{\mu\tau} \rho_{\tau\mu}}{16\pi^2} \left[ \frac{(\log \frac{m_H^2}{m_\tau^2} - \frac{3}{2})}{m_H^2} - \frac{\log(\frac{m_A^2}{m_\tau^2} - \frac{3}{2})}{m_A^2} \right]. \quad (29)$$

At the one-loop level, the diagrams with the Higgs LFC coupling can also give the contributions to the muon g-2, especially for a large lepton Yukawa coupling [37]. The corresponding Feynman diagrams can be obtained by replacing  $\tau$  in the initial state and loop with  $\mu$  in Fig. 2 (a) as well as replacing the initial state  $\tau$  with  $\mu$  and  $\nu_\tau$  in the loop with  $\nu_\mu$  in Fig. 2 (b). The contributions from the one-loop diagrams with the Higgs LFC coupling are given as

$$\Delta a_{\mu 1}^{LFC} = \frac{1}{8\pi^2} \sum_{\phi=h, H, A, H^\pm} |y_{\phi\mu\mu}|^2 r_{\phi\mu} f_\phi(r_{\phi\mu}), \quad (30)$$

where  $r_{\phi\mu} = m_\mu^2/m_\phi^2$  and  $y_{H^\pm\mu\mu} = y_{A\mu\mu}$ . For  $r_{\phi\mu} \ll 1$ ,

$$f_{h,H}(r) \simeq -\ln r - 7/6, \quad f_A(r) \simeq \ln r + 11/6, \quad f_{H^\pm}(r) \simeq -1/6. \quad (31)$$

The muon g-2 can be corrected by the two-loop Barr-Zee diagrams with the fermions loops by replacing the initial state  $\tau$  with  $\mu$  in Fig. 2 (c). Further replacing the fermion loop with  $W$  loop, we obtain the two-loop Barr-Zee diagrams with  $W$  loop which can contribute to muon g-2 for the SM-like Higgs  $h$  as the mediator in the exact alignment limit. Using the well-known classical formulates in [38], the main contributions of two-loop Barr-Zee diagrams in the exact alignment limit are given as

$$\begin{aligned} \delta a_{\mu 2} = & -\frac{\alpha m_\mu}{4\pi^3 m_f} \sum_{\phi=h, H, A; f=t, b, \tau} N_f^c Q_f^2 y_{\phi\mu\mu} y_{\phi ff} F_\phi(x_{f\phi}) \\ & + \frac{\alpha m_\mu}{8\pi^3 v} \sum_{\phi=h} y_{\phi\mu\mu} g_{\phi WW} \left[ 3F_H(x_{W\phi}) + \frac{23}{4}F_A(x_{W\phi}) \right. \\ & \left. + \frac{3}{4}G(x_{W\phi}) + \frac{m_\phi^2}{2m_W^2} \{F_H(x_{W\phi}) - F_A(x_{W\phi})\} \right], \end{aligned} \quad (32)$$

where  $x_{f\phi} = m_f^2/m_\phi^2$ ,  $x_{W\phi} = m_W^2/m_\phi^2$ ,  $g_{hWW} = 1$  and

$$G(y) = -\frac{y}{2} \int_0^1 dx \frac{1}{x(1-x)-y} \left[ 1 - \frac{y}{x(1-x)-y} \log \frac{x(1-x)}{y} \right]. \quad (33)$$

The experimental value of muon g-2 excess is [39]

$$\delta a_\mu = (26.2 \pm 8.5) \times 10^{-10}. \quad (34)$$

## (5) Higgs searches experiments.

- (i) Non-observation of additional Higgs bosons. We employ **HiggsBounds-4.3.1** [40] to implement the exclusion constraints from the neutral and charged Higgses searches at LEP, Tevatron and LHC at 95% confidence level.
- (ii) The global fit to the 125 GeV Higgs signal data. In the exact alignment limit, the SM-like Higgs has the same coupling to the gauge boson and fermions as the Higgs couplings in the SM, which is favored by the 125 GeV Higgs signal data. However, in order to explain the  $\mu\tau$  excess around 125 GeV, we assume that the  $A$  ( $H$ ) almost degenerates with the SM-like Higgs at the 125 GeV. Since the mass splitting of  $A$  ( $H$ ) and  $h$  is smaller than the mass resolution of detector,  $A$  ( $H$ ) can affect the global fit to the 125 GeV Higgs signal data. Following the method in [41], we perform a global fit to the 125 GeV Higgs data of 29 channels, which are given in the appendix A. The signal strength for a channel is defined as

$$\mu_i = \sum_{\hat{H}=h, \phi} \epsilon_{gg\hat{H}}^i R_{gg\hat{H}} + \epsilon_{VBF\hat{H}}^i R_{VBF\hat{H}} + \epsilon_{V\hat{H}}^i R_{V\hat{H}} + \epsilon_{t\bar{t}\hat{H}}^i R_{t\bar{t}\hat{H}}. \quad (35)$$

Where  $R_j = (\sigma \times BR)_j / (\sigma \times BR)_j^{SM}$  with  $j$  denoting the partonic process  $gg\hat{H}$ ,  $VBF\hat{H}$ ,  $V\hat{H}$ , or  $t\bar{t}\hat{H}$ .  $\epsilon_j^i$  denotes the assumed signal composition of the partonic process  $j$ . If  $A$  ( $H$ ) almost degenerates with the SM-like Higgs,  $\phi$  denotes  $A$  ( $H$ ). For an uncorrelated observable  $i$ ,

$$\chi_i^2 = \frac{(\mu_i - \mu_i^{exp})^2}{\sigma_i^2}, \quad (36)$$

where  $\mu_i^{exp}$  and  $\sigma_i$  denote the experimental central value and uncertainty for the  $i$ -channel. We retain the uncertainty asymmetry in the calculation. For the two correlated observables, we take

$$\chi_{i,j}^2 = \frac{1}{1 - \rho^2} \left[ \frac{(\mu_i - \mu_i^{exp})^2}{\sigma_i^2} + \frac{(\mu_j - \mu_j^{exp})^2}{\sigma_j^2} - 2\rho \frac{(\mu_i - \mu_i^{exp})(\mu_j - \mu_j^{exp})}{\sigma_i \sigma_j} \right], \quad (37)$$

where  $\rho$  is the correlation coefficient. We sum over  $\chi^2$  in the 29 channels, and pay particular attention to the surviving samples with  $\chi^2 - \chi_{\min}^2 \leq 6.18$ , where  $\chi_{\min}^2$  denotes the minimum of  $\chi^2$ . These samples correspond to the 95.4% confidence level region in any two-dimension plane of the model parameters when explaining the Higgs data (corresponding to the  $2\sigma$  range).

- (iii) The Higgs decays into  $\tau\mu$ . In the exact alignment limit, the  $\mu\tau$  excess around 125 GeV is from  $A$  ( $H$ )  $\rightarrow \tau\mu$  where  $A$  ( $H$ ) almost degenerates with the SM-like Higgs.

The width of  $A(H) \rightarrow \mu\tau$  is given by

$$\Gamma(A(H) \rightarrow \mu\tau) = \frac{(\rho_{\mu\tau}^2 + \rho_{\tau\mu}^2)m_{A(H)}}{16\pi}. \quad (38)$$

We take the best fit value of  $Br(h \rightarrow \mu\tau) = (0.84_{-0.37}^{+0.39})\%$  based on the CMS search for the  $h \rightarrow \mu\tau$  at the LHC run-I. Since the  $\mu\tau$  excess is assumed to be from the  $A(H)$ , we require the production rates of  $pp \rightarrow A(H) \rightarrow \mu\tau$  to vary from  $\sigma(pp \rightarrow h) \times 0.1\%$  to  $\sigma(pp \rightarrow h) \times 1.62\%$ .

In addition, the CMS collaboration did not publish the bound on the heavy Higgs decaying into  $\mu\tau$ . Ref. [7] gave the bound on the production rate of  $pp \rightarrow \phi \rightarrow \mu\tau$  by recasting results from the original  $h \rightarrow \mu\tau$  analysis of CMS.

## B. Results and discussions

In Fig. 4, we project the surviving samples on the planes of  $\rho_{\tau\mu}$  versus  $\kappa_\ell$  and  $\kappa_u$  versus  $\rho_{\tau\mu}$ . The lower panels show the  $\kappa_u$  is required to be smaller than 1 due to the constraints of  $B$ -meson decays and  $R_b$ . The upper panels show that there is a strong correlation between  $\rho_{\tau\mu}$  and  $\kappa_\ell$ , which is mainly due to the constraints of  $Br(\tau \rightarrow 3\mu)$  on the product  $|\rho_{\tau\mu} \times \kappa_\ell|$ , and obviously affected by the constraints of  $Br(\tau \rightarrow \mu\gamma)$ . For example, in the case of  $m_A = 126$  GeV,  $|\rho_{\tau\mu}|$  is required to be smaller than 0.06 for  $\kappa_\ell = -10$ .

In the case of  $m_A = 126$  GeV, there are two different regions where the muon g-2 anomaly can be explained. (i)  $\rho_{\tau\mu} = 0$  and  $|\kappa_\ell| > 100$ : The Higgs LFV couplings are absent due to  $\rho_{\tau\mu} = 0$ , and the muon g-2 can be only corrected via the diagrams with the Higgs LFC couplings. Without the contributions of top quark loops, the contributions of the CP-even (CP-odd) Higgs to muon g-2 are negative (positive) at the two-loop level and positive (negative) at one-loop level. As  $m_f^2/m_\mu^2$  could easily overcome the loop suppression factor  $\alpha/\pi$ , the two-loop contributions may be larger than one-loop ones. Therefore, the muon g-2 can obtain the positive contributions from  $A$  loop and negative contributions from  $H$  loop. For the enough mass splitting of  $H$  and  $A$ , the muon g-2 can be sizably enhanced by the diagrams with the large Higgs LFC couplings. The corresponding  $\kappa_u$  is required to be smaller than 0.2 due to the constraints of the search for  $gg \rightarrow A \rightarrow \tau\bar{\tau}$  at the LHC, see the pluses (red) with  $\rho_{\tau\mu} = 0$  shown in the lower-left panel of Fig. 4. (ii)  $0.04 < |\rho_{\tau\mu}| < 0.18$  and  $-9 < \kappa_\ell < 3$ : The muon g-2 can be corrected by the diagrams

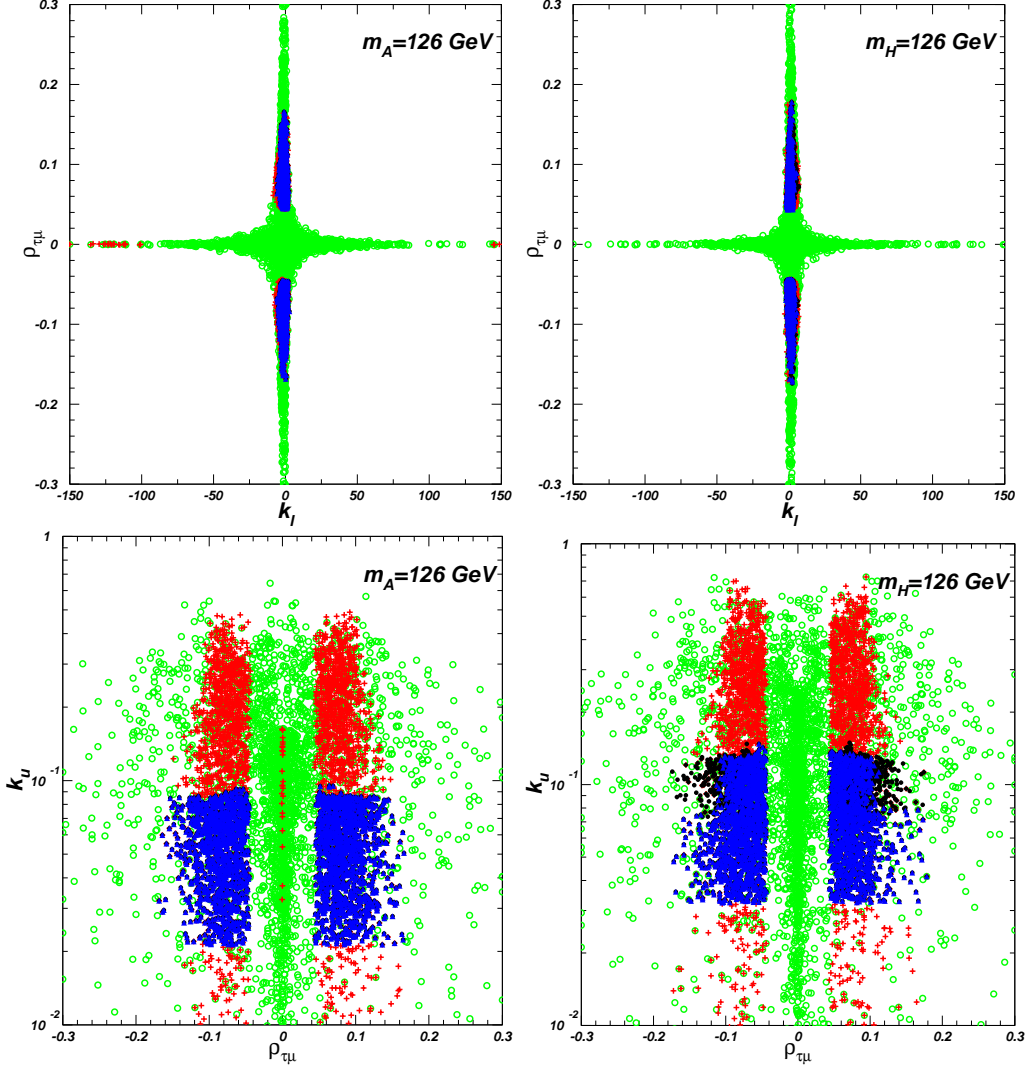


FIG. 4: The surviving samples projected on the planes of  $\rho_{\tau\mu}$  versus  $\kappa_\ell$  and  $\kappa_u$  versus  $\rho_{\tau\mu}$ . The circles (green) are allowed by the "pre-muon g-2" constraints: theoretical constraints, precision electroweak data,  $R_b$ ,  $B$  meson decays,  $\tau$  decays, the exclusion limits of Higgses, and the 125 GeV Higgs data; the pluses (red) allowed by the pre-muon g-2 and muon g-2 excess; the bullets (black) and triangles (blue) allowed by the pre-muon g-2, the muon g-2 anomaly and  $\mu\tau$  excess around 125 GeV, and the triangles (blue) further allowed by the experimental constraints of the heavy Higgs decaying into  $\mu\tau$ .

with the Higgs LFV interactions and the Higgs LFC interactions, and the contributions of the former dominate over those of the latter due to the small  $|\kappa_\ell|$ . For the diagrams with the Higgs LFV couplings, the muon g-2 obtains the positive contributions from  $A$  loop and negative contributions from  $H$  loop due to  $\rho_{\mu\tau} = -\rho_{\tau\mu}$ . For the enough mass splitting of  $H$

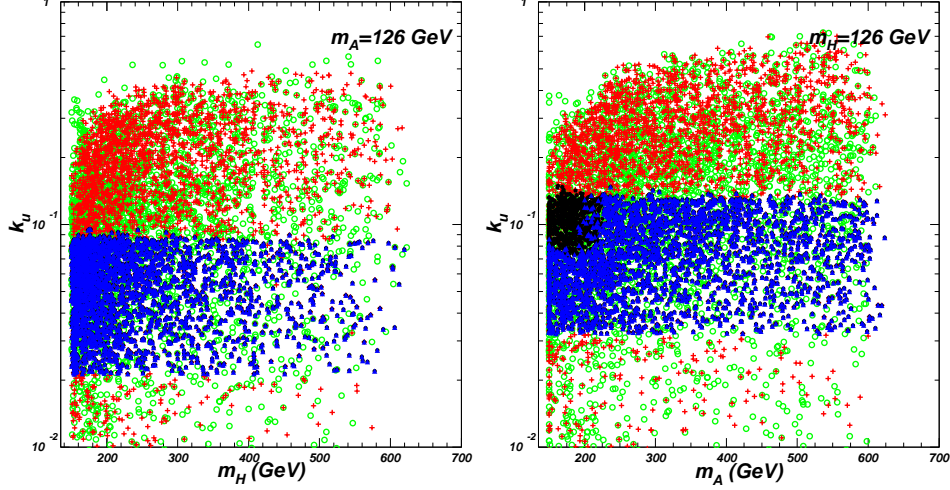


FIG. 5: Same as Fig. 4, but  $\kappa_u$  versus  $m_H$  and  $\kappa_u$  versus  $m_A$ .

and  $A$ , the muon  $g-2$  can be sizably enhanced by the diagrams with the large Higgs LFV couplings, and slightly corrected by those with the Higgs LFC couplings.

In the case of  $m_H = 126$  GeV, the contributions of the CP-even Higgs dominate over those of the CP-odd Higgs due to  $m_A > m_H$ . The muon  $g-2$  obtains the negative contributions from the diagrams with the Higgs LFC couplings and positive contributions from the diagrams with the LFV couplings due to  $\rho_{\mu\tau} = \rho_{\tau\mu}$ . Therefore, a proper  $\rho_{\tau\mu}$  is required to explain the muon  $g-2$  excess,  $0.04 < |\rho_{\tau\mu}| < 0.18$  and  $-3 < \kappa_\ell < 8$  as shown in the right panels of Fig. 4.

In the case of  $m_A = 126$  GeV,  $0.02 < \kappa_u < 0.1$  is favored by the  $\mu\tau$  excess around 125 GeV and allowed by the experimental constraints of the heavy Higgs decaying into  $\mu\tau$ . In the case of  $m_H = 126$  GeV,  $0.03 < \kappa_u < 0.15$  is favored by the  $\mu\tau$  excess around 125 GeV, but some samples with a relatively large  $\kappa_u$  are excluded by the experimental constraints of the heavy Higgs decaying into  $\mu\tau$ . As well known, the effective  $ggA$  coupling is larger than the  $ggH$  coupling for the same Yukawa couplings and Higgs masses since the form factor of CP-odd Higgs loop is larger than the CP-even Higgs loop. Thus,  $\kappa_u$  in the case of  $m_H = 126$  GeV is required to be larger than that in the case of  $m_A = 126$  GeV in order to obtain the correct  $\mu\tau$  excess around 125 GeV.  $\sigma(pp \rightarrow A \rightarrow \mu\tau)$  in the case of  $m_H = 126$  GeV ( $A$  as the heavy Higgs) is much larger than  $\sigma(pp \rightarrow H \rightarrow \mu\tau)$  in the case of  $m_A = 126$  GeV ( $H$  as the heavy Higgs) due to the enhancements of the large top Yukawa coupling and the form factor of the CP-odd Higgs. Therefore, the experimental data of the heavy Higgs decaying into  $\mu\tau$  give more strong constraints on the case of  $m_H = 126$  GeV than the case of  $m_A = 126$  GeV.

In Fig. 5, we project the surviving samples on the plane of  $\kappa_u$  versus  $m_A$  ( $m_H$ ) in the case of  $m_H = 126$  GeV ( $m_A = 126$  GeV). The upper bound of  $\sigma(pp \rightarrow A/H \rightarrow \mu\tau)$  is taken from Ref. [7], which is obtained by recasting results from the original CMS  $h \rightarrow \mu\tau$  analysis for the heavy Higgs in the range of 125 GeV and 275 GeV. From the right panel, for the case of  $m_H = 126$  GeV we find that the experimental data of the heavy Higgs decaying into  $\mu\tau$  can exclude most samples in the ranges of  $0.07 < \kappa_u < 0.15$  and  $m_A < 230$  GeV, which can explain the excesses of muon g-2 and  $\mu\tau$  around 125 GeV. For  $m_A > 230$  GeV, all the surviving samples which are consistent with the  $\mu\tau$  excess around 125 GeV are allowed by the experimental constraints of the heavy Higgs decaying into  $\mu\tau$ . As discussed before, the left panel shows that all the surviving samples are allowed by the experimental constraints of the heavy Higgs decaying into  $\mu\tau$  in the case of  $m_A = 126$  GeV.

Note that there is the  $\kappa_\ell$  asymmetry in the regions of  $0.04 < |\rho_{\tau\mu}| < 0.18$ ,  $-9 < \kappa_\ell < 3$  and  $0.02 < \kappa_u < 0.1$  for  $m_A = 126$  GeV where muon g-2 can be explained. The main reason is from the constraints of  $\tau \rightarrow \mu\gamma$ . In the above regions, the top quark can give sizable contributions to  $\tau \rightarrow \mu\gamma$  via the " $A_{2L}$ " and " $A_{2R}$ " terms as shown in Eq. (24), which have destructive (constructive) interferences with the " $A_{1L0}$ " of Eq. (20) and " $A_{1R0}$ " of Eq. (22) induced by the one-loop contributions of  $\tau$  for  $\kappa_\ell < 0$  ( $\kappa_\ell > 0$ ). Therefore,  $|\kappa_\ell|$  for  $\kappa_\ell < 0$  is allowed to be much larger than that for  $\kappa_\ell > 0$ . Similar reason is for the  $\kappa_\ell$  asymmetry in the case of  $m_H = 126$  GeV but the destructive (constructive) interferences for  $\kappa_\ell > 0$  ( $\kappa_\ell < 0$ ).

In Fig. 6, we project the surviving samples on the planes of  $\rho_{\tau\mu}$  versus  $m_H$  and  $\rho_{\tau\mu}$  versus  $m_A$  in the cases of  $m_A = 126$  GeV and  $m_H = 126$  GeV, respectively. We find that  $\rho_{\tau\mu}$  is sensitive to the mass of heavy Higgs, and the absolute value decreases with increasing of the mass of heavy Higgs in order to explain the muon g-2 anomaly and the  $\mu\tau$  excess around 125 GeV. As we discussed above, there is an opposite sign between the contributions of the  $H$  loops and  $A$  loops to the muon g-2. Therefore, with the decreasing of the mass splitting of  $H$  and  $A$ , the cancelation between the contributions of  $H$  and  $A$  loops becomes sizable so that a large absolute value of  $\rho_{\mu\tau}$  is required to enhance the muon g-2.

In Fig. 7, we project the surviving samples on the planes of  $m_{H^\pm}$  versus  $m_H$  and  $m_{H^\pm}$  versus  $m_A$  in the cases of  $m_A = 126$  GeV and  $m_H = 126$  GeV, respectively. We find that the mass splitting of  $H^\pm$  and  $H$  ( $A$ ) decreases with increasing of  $m_{H^\pm}$  in the case of  $m_A = 126$  GeV ( $m_H = 126$  GeV), which is due to the constraints of the oblique parameters and  $\delta\rho$ .



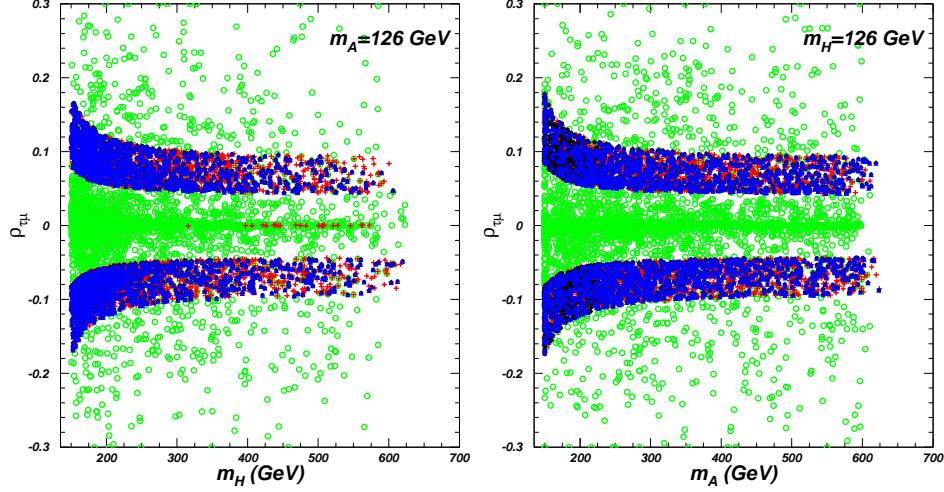


FIG. 6: Same as Fig. 4, but  $\rho_{\tau\mu}$  versus  $m_H$  and  $\rho_{\tau\mu}$  versus  $m_A$ .

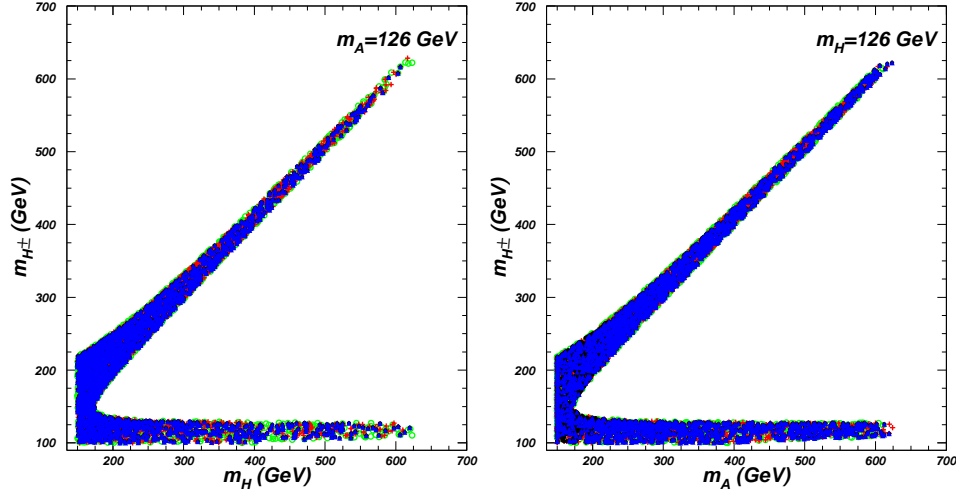


FIG. 7: Same as Fig. 4, but  $m_{H^\pm}$  versus  $m_H$  and  $m_{H^\pm}$  versus  $m_A$ .

However, for  $m_{H^\pm} < 130$  GeV,  $m_H$  ( $m_A$ ) is allowed to be as large as 625 GeV in the case of  $m_A = 126$  GeV ( $m_H = 126$  GeV).

In this paper we focus on the exact alignment limit. If the alignment limit is approximately realized, the  $\mu\tau$  excess can be from the SM-like Higgs ( $h$ ) in addition to  $H$  or  $A$  around the 125 GeV. Therefore, the upper limits of  $\kappa_u$  become more stringent. When the  $\mu\tau$  excess is mainly from  $h$ , the lower limit of  $\kappa_u$  will disappear since the  $h t \bar{t}$  coupling hardly changes with  $\kappa_u$ , and the  $A(H) t \bar{t}$  coupling is (nearly) proportional to  $\kappa_u$ . In addition, the upper limit of  $\rho_{\mu\tau}$  can become more strong for the proper deviation from the alignment limit. For example, for  $\sin(\beta - \alpha) = 0.996$ ,  $Br(h \rightarrow \mu\tau) < 1.62\%$  will give an upper limit of  $|\rho_{\mu\tau}| < 0.0408$ , which is much smaller than that in the exact alignment limit. In the exact

alignment limit, the widths of  $H \rightarrow hh$ ,  $WW^{(*)}$ ,  $ZZ^{(*)}$  and  $A \rightarrow hZ$  are equal to zero, and increase with decreasing of  $|\sin(\beta-\alpha)|$ . Therefore, the searches for  $H \rightarrow hh$ ,  $WW^{(*)}$ ,  $ZZ^{(*)}$  and  $A \rightarrow hZ$  can be used to probe the deviation from the alignment limit. These signatures refer to the  $H$  or  $A$  whose mass is not near 125 GeV. Otherwise, its signal would be indistinguishable from that coming from the SM-like light Higgs, and even  $H \rightarrow hh$  ( $A \rightarrow hZ$ ) is absent for  $H$  ( $A$ ) near 125 GeV. Some similar studies have been done in the singlet extension of the SM [42].

In the previous studies, the  $\mu\tau$  excess is assumed to be from the SM-like Higgs  $h$ . In this paper we discuss another interesting scenario where the  $\mu\tau$  excess is from either  $H$  or  $A$  near the observed Higgs signal. There is no  $AVV$  coupling due to the CP-conserving. The  $HVV$  coupling is absent and the  $hVV$  coupling is the same as the SM value in the exact alignment limit. Therefore, the two scenarios can be distinguished by observing the  $\mu\tau$  signal via the vector boson fusion production process at the LHC with high integrated luminosity. In other words, if the  $\mu\tau$  signal excess is observed in the gluon fusion process and not observed in the vector boson fusion process, the scenario in this paper will be strongly favored. Even when  $\sin(\beta-\alpha)$  deviates from the alignment limit sizably, the production rates of  $\mu\tau$  signal via the gluon fusion and vector boson fusion can still have different correlations in the two different scenarios.

#### IV. CONCLUSION

In this paper we examine the muon g-2 anomaly and the  $\mu\tau$  excess around 125 GeV in the exact alignment limit of 2HDM. In the scenario, the SM-like Higgs couplings to the SM particles are the same as the Higgs couplings in the SM at the tree level, and the tree-level LFV coupling  $h\mu\tau$  is absent. We assume the  $\mu\tau$  signal excess observed by CMS to be respectively from the  $H$  and  $A$ , which almost degenerates with the SM-like Higgs at the 125 GeV. After imposing various relevant theoretical constraints and experimental constraints from precision electroweak data,  $B$ -meson decays,  $\tau$  decays and Higgs searches, we obtain the following observations:

For the case of  $m_A = 126$  GeV, the muon g-2 anomaly can be explained in two different regions: (i)  $\rho_{\tau\mu} = 0$  and  $|\kappa_\ell| > 100$ ; (ii)  $0.04 < |\rho_{\tau\mu}| < 0.18$  ( $|\rho_{\tau\mu}|$  is sensitive to  $m_H$ ) and  $-9 < \kappa_\ell < 3$ . Further, the  $\mu\tau$  excess around 125 GeV can be explained in the region (ii) with

$0.02 < \kappa_u < 0.1$  where all the surviving samples are allowed by the experimental constraints of the heavy Higgs decaying into  $\mu\tau$ .

For the case of  $m_H = 126$  GeV, the muon g-2 anomaly excludes the region of  $\rho_{\tau\mu} = 0$ , and can be only explained in the region with a proper  $\rho_{\tau\mu}$ . The muon g-2 anomaly and  $\mu\tau$  excess favor  $0.04 < |\rho_{\tau\mu}| < 0.18$  ( $|\rho_{\tau\mu}|$  is sensitive to  $m_A$ ),  $-3 < \kappa_\ell < 8$  and  $0.03 < \kappa_u < 0.15$ . However, most samples in the ranges of  $0.07 < \kappa_u < 0.15$  and  $m_A < 230$  GeV are further excluded by the experimental constraints of the heavy Higgs decaying into  $\mu\tau$ .

### Acknowledgment

This work has been supported by the National Natural Science Foundation of China under grant Nos. 11575152, 11375248.

### Appendix A: The measured values of the signal strengths of 125 GeV Higgs at the LHC and Tevatron.

- 
- [1] ATLAS Collaboration, JHEP **1511**, 211 (2015).
  - [2] ATLAS Collaboration, arXiv:1604.07730.
  - [3] CMS Collaboration, Phys. Lett. B **749**, 337-362 (2015).
  - [4] CMS Collaboration, "Search for Lepton Flavour Violating Decays of the Higgs Boson in the mu-tau final state at 13 TeV," CMS-PAS-HIG-16-005.
  - [5] I. Dorsner, S. Fajfer, A. Greljo, J. F. Kamenik, N. Kosnik and I. Nisandzic, JHEP **06**, 108 (2015); A. Crivellin, G. D'Ambrosio, J. Heeck, Phys. Rev. Lett. **114**, 151801 (2015); Y. Omura, E. Senaha, K. Tobe, JHEP **1505**, 028 (2015); S. P. Das, J. H.-Sanchez, A. Rosado and R. Xoxocotzi, arXiv:1503.01464; C. X. Yue, C. Pang and Y. C. Guo, J. Phys. G **42**, 075003 (2015); A. Crivellin, J. Heeck and P. Stoffer, Phys. Rev. Lett. **116**, 081801 (2016); F. J. Botella, G. C. Branco, M. Nebot and M. N. Rebelo, arXiv:1508.05101; R. Benbrik, C.-H. Chen, T. Nomura, arXiv:1511.08544; D. A. Sierra, A. Vicente, Phys. Rev. D **90**, 115004 (2014); J. Heeck, M. Holthausen, W. Rodejohann, Y. Shimizu, Nucl. Phys. B **896**, 281-310 (2015); I. d. M. Varzielas, O. Fischer, V. Maurer, JHEP **08**, 080 (2015); X. Liu, L. Bian, X.

TABLE I: The measured values of the signal strengths of  $h \rightarrow \gamma\gamma$  at the LHC and Tevatron. The composition  $\epsilon_j^i$  of each production mode in each data are given.

| Channel   | Signal strength $\mu$   | $M_H(\text{GeV})$ | Production mode |      |      |      |
|---|-------------------------|-------------------|-----------------|------|------|------|
|   |                         |                   | ggF             | VBF  | VH   | ttH  |
| ATLAS (20.3fb <sup>-1</sup> at 8TeV) [43]       |                         |                   |                 |      |      |      |
| $\mu_{ggH}$                                     | $1.32 \pm 0.38$         | 125.40            | 100%            | -    | -    | -    |
| $\mu_{VBF}$                                     | $0.8 \pm 0.7$           | 125.40            | -               | 100% | -    | -    |
| $\mu_{WH}$                                      | $1.0 \pm 1.6$           | 125.40            | -               | -    | 100% | -    |
| $\mu_{ZH}$                                      | $0.1^{+3.7}_{-0.1}$     | 125.40            | -               | -    | 100% | -    |
| $\mu_{ttH}$                                     | $1.6^{+2.7}_{-1.8}$     | 125.40            | -               | -    | -    | 100% |
| CMS (19.7fb <sup>-1</sup> at 8TeV) [44]         |                         |                   |                 |      |      |      |
| $\mu_{ggH}$                                     | $1.12^{+0.37}_{-0.32}$  | 124.70            | 100%            | -    | -    | -    |
| $\mu_{VBF}$                                     | $1.58^{+0.77}_{-0.68}$  | 124.70            | -               | 100% | -    | -    |
| $\mu_{VH}$                                      | $-0.16^{+1.16}_{-0.79}$ | 124.70            | -               | -    | 100% | -    |
| $\mu_{ttH}$                                     | $2.69^{+2.51}_{-1.81}$  | 124.70            | -               | -    | -    | 100% |
| Tevatron (10.0fb <sup>-1</sup> at 1.96TeV) [45] |                         |                   |                 |      |      |      |
| Combined  | $6.14^{+3.25}_{-3.19}$  | 125               | 78%             | 5%   | 17%  | -    |

TABLE II: The same as Table I but for  $H \rightarrow ZZ^{(*)}$ .

| Channel                                       | Signal strength $\mu$                  | $M_H(\text{GeV})$ | Production mode |      |      |      |
|---|--|-------------------|-----------------|------|------|------|
|   |  |                   | ggF             | VBF  | VH   | ttH  |
| ATLAS (20.3fb <sup>-1</sup> at 8TeV) [46, 47] |  |                   |                 |      |      |      |
| Inclusive                                     | 1.66 <sup>+0.45</sup> <sub>-0.38</sub> | 124.51            | 87.5%           | 7.1% | 4.9% | 0.5% |
| CMS (19.7fb <sup>-1</sup> at 8TeV) [48]       |  |                   |                 |      |      |      |
| Inclusive                                     | 0.93 <sup>+0.29</sup> <sub>-0.25</sub> | 125.6             | 87.5%           | 7.1% | 4.9% | 0.5% |

Q. Li and J. Shu, arXiv:1508.05716; X.-F. Han, L. Wang, J. M. Yang, Phys. Lett. B **757**, 537-547 (2016); D. Das, A. Kundu, Phys. Rev. D **92**, 015009 (2015); F. J. Botella, G. C. Branco, M. Nebot and M. N. Rebelo, Eur. Phys. Jour. C **76**, 161 (2016); A. E. Carcamo Hernandez, I. de Medeiros Varzielas and E. Schumacher, Phys. Rev. D **93**, 016003 (2016); S. Banerjee,

TABLE III: The same as Table I but for  $H \rightarrow WW^{(*)}$ .

| Channel   | Signal strength $\mu$                  | $M_H(\text{GeV})$ | Production mode |      |      |      |
|---|--|-------------------|-----------------|------|------|------|
|   |  |                   | ggF             | VBF  | VH   | ttH  |
| ATLAS (20.7fb <sup>-1</sup> at 8TeV) [49]       |  |                   |                 |      |      |      |
| Inclusive                                       | 0.99 ± 0.30                            | 125               | 87.5%           | 7.1% | 4.9% | 0.5% |
| CMS (19.4fb <sup>-1</sup> at 8TeV) [50]         |  |                   |                 |      |      |      |
| 0/1 jet   | 0.74 <sup>+0.22</sup> <sub>-0.20</sub> | 125.6             | 97%             | 3%   | -    | -    |
| VBF tag   | 0.60 <sup>+0.57</sup> <sub>-0.46</sub> | 125.6             | 17%             | 83%  | -    | -    |
| VH tag (2l2ν2j)                                 | 0.39 <sup>+1.97</sup> <sub>-1.87</sub> | 125.6             | -               | -    | 100% | -    |
| WH tag (3l3ν)                                   | 0.56 <sup>+1.27</sup> <sub>-0.95</sub> | 125.6             | -               | -    | 100% | -    |
| Tevatron (10.0fb <sup>-1</sup> at 1.96TeV) [45] |  |                   |                 |      |      |      |
| Combined  | 0.85 <sup>+0.88</sup> <sub>-0.81</sub> | 125               | 78%             | 5%   | 17%  | -    |

 TABLE IV: The same as Table I but for  $H \rightarrow b\bar{b}$ .

| Channel  | Signal strength $\mu$                  | $M_H(\text{GeV})$ | Production mode |     |      |      |
|--|--|-------------------|-----------------|-----|------|------|
|  |  |                   | ggF             | VBF | VH   | ttH  |
| ATLAS (20.3fb <sup>-1</sup> at 8TeV) [51, 52]                                |  |                   |                 |     |      |      |
| VH tag   | 0.2 <sup>+0.7</sup> <sub>-0.6</sub>    | 125.5             | -               | -   | 100% | -    |
| ttH tag  | 1.8 <sup>+1.66</sup> <sub>-1.57</sub>  | 125.4             | -               | -   | -    | 100% |
| CMS (18.9fb <sup>-1</sup> at 8TeV) [53], (19.5fb <sup>-1</sup> at 8TeV) [54] |  |                   |                 |     |      |      |
| VH tag   | 1.0 ± 0.5                              | 125               | -               | -   | 100% | -    |
| ttH tag  | 0.67 <sup>+1.35</sup> <sub>-1.33</sub> | 125               | -               | -   | -    | 100% |
| Tevatron (10.0fb <sup>-1</sup> at 1.96TeV) [55]                              |  |                   |                 |     |      |      |
| VH tag   | 1.59 <sup>+0.69</sup> <sub>-0.72</sub> | 125               | -               | -   | 100% | -    |

B. Bhattacharjee, M. Mitra, M. Spannowsky, arXiv:1603.05952; M. Sher, K. Thrasher, Phys. Rev. D **93**, 055021 (2016); J. G. Korner, A. Pilaftsis, K. Schilcher, Phys. Lett. B **285**, 68 (1992); Phys. Rev. D **47**, 1080 (1993).

[6] Y. Omura, E. Senaha, K. Tobe, arXiv:1511.08880.

[7] M. Buschmann, J. Kopp, J. Liu, X.-P. Wang, arXiv:1601.02616.

TABLE V: The same as Table I but for  $H \rightarrow \tau\tau$ . The correlation for the  $\tau\tau$  data of ATLAS is  $\rho = -0.51$ .

| Channel                                   | Signal strength $\mu$ | $M_H(\text{GeV})$ | Production mode |       |       |     |
|---|-----------------------|-------------------|-----------------|-------|-------|-----|
|   |                       |                   | ggF             | VBF   | VH    | ttH |
| ATLAS (20.3fb <sup>-1</sup> at 8TeV) [56] |                       |                   |                 |       |       |     |
| $\mu(ggF)$                                | $1.1^{+1.3}_{-1.0}$   | 125               | 100%            | -     | -     | -   |
| $\mu(VBF + VH)$                           | $1.6^{+0.8}_{-0.7}$   | 125               | -               | 59.6% | 40.4% | -   |
| CMS (19.7fb <sup>-1</sup> at 8TeV) [57]   |                       |                   |                 |       |       |     |
| 0 jet                                     | $0.34 \pm 1.09$       | 125               | 96.9%           | 1.0%  | 2.1%  | -   |
| 1 jet                                     | $1.07 \pm 0.46$       | 125               | 75.7%           | 14.0% | 10.3% | -   |
| VBF tag                                   | $0.94 \pm 0.41$       | 125               | 19.6%           | 80.4% | -     | -   |
| VH tag                                    | $-0.33 \pm 1.02$      | 125               | -               | -     | 100%  | -   |

- [8] J. Heeck, M. Holthausen, W. Rodejohann and Y. Shimizu, Nucl. Phys. B **896**, 281-310 (2015); M. D. Campos, A. E. C. Hernandez, H. Pas and E. Schumacher, Phys. Rev. D **91**, 116011 (2015); D. Aloni, Y. Nir and E. Stamou, JHEP **04**, 162 (2016); X.-G. He, J. Tandean and Y.-J. Zheng, JHEP **09**, 093 (2015); K. Cheung, W.-Y. Keung and P.-Y. Tseng, Phys. Rev. D **93**, 015010 (2016); C.-F. Chang, C.-H. Vincent Chang, C. S. Nugroho, T.-C. Yuan, arXiv:1602.00680; C.-H. Chen, T. Nomura, arXiv:1602.07519; C. Alvarado, R. M. Capdevilla, A. Delgado, A. Martin, arXiv:1602.08506; S. Baek, T. Nomura, H. Okada, Phys. Lett. B **759**, 91-98 (2016); J. Herrero-Garcia, N. Rius, A. Santamaria, arXiv:1605.06091; K. H. Phan, H. T. Hung, L. T. Hue, arXiv:1605.07164; W. Altmannshofer, M. Carena, A. Crivellin, arXiv:1604.08221; K. Huitu, V. Keus, N. Koivunen, O. Lebedev, JHEP **1605**, 026 (2016); S. Baek and K. Nishiwaki, Phys. Rev. D **93**, 015002 (2016); B. Yang, J. Han, N. Liu, arXiv:1605.09248; E. Arganda, M. J. Herrero, X. Marcano, C. Weiland Phys. Rev. D **93**, 055010 (2016); S. Baek, Z.-F. Kang, JHEP **1603**, 106 (2016).
- [9] J. Bernon, J. F. Gunion, H. E. Haber, Y. Jiang and S. Kraml, Phys. Rev. D **92**, 075004 (2015).
- [10] J. F. Gunion, H. E. Haber, Phys. Rev. D **67**, 075019 (2003).
- [11] N. Craig, S. Thomas, JHEP **1211**, 083 (2012).
- [12] N. Craig, J. A. Evans, R. Gray, C. Kilic, M. Park, S. Somalwar, S. Thomas, JHEP **1302**,

- 033 (2013).
- [13] N. Craig, J. Galloway, S. Thomas, arXiv:1305.2424.
  - [14] H. E. Haber, arXiv:1401.0152.
  - [15] D. Asner, T. Barklow, C. Calancha, K. Fujii, N. Graf, H. E. Haber et al., arXiv:1310.0763.
  - [16] G. Bhattacharyya, D. Das, P. B. Pal, M. N. Rebelo, JHEP **1310**, 081 (2013); G. Bhattacharyya, D. Das, Phys. Rev. D **91**, 015005 (2015).
  - [17] P. S. Bhupal Dev, A. Pilaftsis, JHEP **12**, 024 (2014).
  - [18] M. Carena, I. Low, N. R. Shah, C. E. M. Wagner, JHEP **1404**, 015 (2014).
  - [19] M. Carena, H. E. Haber, I. Low, N. R. Shah, C. E. M. Wagner, Phys. Rev. D **91**, 035003 (2015).
  - [20] P. Bechtle, H. E. Haber, S. Heinemeyer, O. Stål, T. Stefaniak, G. Weiglein, L. Zeune, arXiv:1608.00638.
  - [21] R. A. Battye, G. D. Brawn, A. Pilaftsis, JHEP **1108**, 020 (2011).
  - [22] S. Davidson, H. E. Haber, Phys. Rev. D **72**, 035004 (2005); Phys. Rev. D **72**, 099902 (2005).
  - [23] A. Pich, P. Tuzon, Phys. Rev. D **80**, 091702 (2009).
  - [24] V. Barger, L. L. Everett, H. E. Logan, and G. Shaughnessy, Phys. Rev. D **88**, 115003 (2013).
  - [25] D. Eriksson, J. Rathsman, O. Stål, Comput. Phys. Commun. **181**, 189 (2010); Comput. Phys. Commun. **181**, 833 (2010).
  - [26] C. Q. Geng and J. N. Ng, Phys. Rev. D **38**, 2857 (1988) [Erratum-ibid. D 41, 1715 (1990)].
  - [27] M. Misiak, H. M. Asatrian, R. Boughezal, M. Czakon, T. Ewerth, A. Ferroglia, P. Fiedler, and P. Gambino et al., Phys. Rev. Lett. **114**, 221801 (2015).
  - [28] X.-Q. Li, J. Lu, A. Pich, JHEP **1406**, 022 (2014).
  - [29] H. E. Haber, H. E. Logan, Phys. Rev. D **62**, 015011 (2010); G. Degrandi, P. Slavich, Phys. Rev. D **81**, 075001 (2010); W. Su, J. M. Yang, Phys. Lett. B **757**, 136 (2016).
  - [30] A. Crivellin, A. Kokulu and C. Greub, Phys. Rev. D **87**, 094031 (2013).
  - [31] K. Hayasaka, Phys. Lett. B **687**, 139-143 (2010).
  - [32] Y. Omura, E. Senaha, K. Tobe, arXiv:1511.08880.
  - [33] K. Hayasaka et al. [Belle Collaboration], Phys. Lett. B **666**, 16 (2008); B. Aubert et al. [BaBar Collaboration], Phys. Rev. Lett. **104**, 021802 (2010).
  - [34] A. Celis, V. Cirigliano, E. Passemar, Phys. Rev. D **89**, 013008 (2014).
  - [35] BaBar Collaboration, B. Aubert et al., Phys. Rev. Lett. **98**, 061803 (2007).

- [36] S. Davidson, G. Grenier, Phys. Rev. D **81**, 095016 (2010); K. A. Assamagan, A. Deandrea and P. A. Delsart, Phys. Rev. D **67**, 035001 (2003).
- [37] B. Lautrup, A. Peterman, E. de Rafael, Phys. Rept. **3**, 193-260 (1972); J. P. Leveille, Nucl. Phys. B **137**, 63 (1978); A. Dedes, H. E. Haber, JHEP **0105**, 006 (2001).
- [38] D. Chang, W. S. Hou and W. Y. Keung, Phys. Rev. D **48**, 217 (1993); V. Ilisie, JHEP **1504**, 077 (2015).
- [39] G. Bennett *et al.* [Muon G-2 Collaboration Collaboration], Phys. Rev. D **73**, 072003 (2006); F. Jegerlehner, A. Nyffeler, Phys. Rept. **477**, 1 (2009); A. Broggio, *et al.*, JHEP **1411**, 058 (2014).
- [40] P. Bechtle, O. Brein, S. Heinemeyer, G. Weiglein, K. E. Williams, Comput. Phys. Commun. **181**, 138-167 (2010); P. Bechtle, O. Brein, S. Heinemeyer, O. Stål, T. Stefaniak, G. Weiglein, K. E. Williams, Eur. Phys. Jour. C **74**, 2693 (2014).
- [41] J. R. Espinosa, C. Grojean, M. Muhlleitner, M. Trott, JHEP **1205**, 097 (2012); G. Belanger, B. Dumont, U. Ellwanger, J. F. Gunion, S. Kraml, JHEP **1302**, 053 (2013); P. P. Giardino, K. Kannike, M. Raidal, A. Strumia, JHEP **1206**, 117 (2012); B. Dumont, S. Fichet, G. Gersdorff, JHEP **1307**, 065 (2013); L. Wang, X.-F. Han, Phys. Rev. D **87**, 015015 (2013); Phys. Rev. D **86**, 095007 (2012); Phys. Lett. B **739**, 416 (2014); J. Cao, *et al.*, JHEP **1203**, 086 (2012); J. S. Lee, P. Y. Tseng, JHEP **1305**, 134 (2013); K. Cheung, J. S. Lee, P.-Y. Tseng, Phys. Rev. D **90**, 095009 (2014).
- [42] T. Robens, T. Stefaniak, Eur. Phys. Jour. C **75**, 105 (2015).
- [43] G. Aad *et al.* [ATLAS Collaboration], arXiv:1408.7084.
- [44] V. Khachatryan *et al.* [CMS Collaboration], arXiv:1407.0558.
- [45] Aurelio Juste, standard model Higgs boson searches at the Tevatron, talk at HCP2012, 15 Nov 2012, Kyoto, Japan,  
<http://kds.kek.jp/conferenceDisplay.py?confId=9237>.
- [46] G. Aad *et al.* [ATLAS Collaboration], arXiv:1406.3827.
- [47] Plenary talk by M. Kado, “Phyiscis of the Brout-Englert-Higgs boson in ATLAS”, ICHEP 2014, Spain.
- [48] S. Chatrchyan *et al.* [CMS Collaboration], Phys. Rev. D **89**, 092007 (2014).
- [49] Talk by C. Mills, “Measurement of Cross Sections and Couplings of the Higgs Boson in the  $WW$  decay Channel using the ATLAS detector”, ICHEP 2014, Spain.



- [50] S. Chatrchyan *et al.* [CMS Collaboration], JHEP **1401**, 096 (2014).
- [51] The ATLAS Collaboration, “Search for the  $b\bar{b}$  decay of the Standard Model Higgs boson in associated W/ZH production with the ATLAS detector,” ATLAS-CONF-2013-079.
- [52] Talk by E. Shabalina, “Search for Higgs Bosons produced in association with top quarks with the ATLAS detector”, ICHEP 2014, Spain.
- [53] S. Chatrchyan *et al.* [CMS Collaboration], Phys. Rev. D **89**, 012003 (2014).
- [54] The CMS Collaboration, “Search for  $t\bar{t}H$  events in the  $H \rightarrow b\bar{b}$  final state using the Matrix Element Method,” CMS-PAS-HIG-14-010.
- [55] Talk by K. Herner, “Studies of the Higgs boson properties at DØ”, ICHEP 2014, Spain.
- [56] The ATLAS Collaboration, Evidence for Higgs Boson Decays to the  $\tau^+\tau^-$  Final State with the ATLAS Detector, ATLAS-CONF-2013-108.
- [57] S. Chatrchyan *et al.* [CMS Collaboration], JHEP **1405**, 104 (2014).